ARTICLE

Microwave-Assisted Hydrothermal Synthesis, Crystal Structure, and Thermal Decomposition of Strontium Citrate Monohydrate $Sr_3(C_6H_5O_7)_2 \cdot H_2O$

Matthias Hämmer,[a] Vivien Wessels,[a] Romy Ettlinger,[a] and Henning. A. Höppe*[a]

Dedicated Prof. Dr. Thomas M. Klapötke on the Occasion of his 60th Birthday

Abstract. Microcrystalline strontium citrate monohydrate $Sr_3(C_6H_5O_7)_2 \cdot H_2O$ was prepared by a microwave-assisted hydrothermal synthesis. Single-crystal X-ray structure determination ($P\bar{1}$, a = 10.0572(4), b = 10.1506(5), c = 10.8531(5) Å, α = 89.642(2)°, β = 67.156(2)°, γ = 62.367(2)°, 3040 independent reflections, 353 refined parameters, wR_2 = 0.066) revealed three different Sr sites coordinated eight-, nine and ten-fold by two crystallographically different citrate molecules with one comprising oriental disorder, but not by the crystal water molecule. These findings are supported by energy dispersive X-ray spectroscopy, powder XRD, infrared spectroscopy and thermal analysis. Further, the latter three methods are applied to the hitherto only strontium citrate hydrate with known crystal structure $Sr_3(C_6H_5O_7)_2 \cdot 5H_2O$ and both compounds are compared, especially with respect to their possible application as precursors.

Introduction

In the course of our systematic investigations on silicate-analogous materials[1–4] we are also interested in suitable precursor compounds.[5,6] Cheap and readily available precursors are often attractive if the morphology of the precursor is passed on to the final product.[5,7] Furthermore, they facilitate new synthesis routes – often at significantly lower temperatures. In this context we came across the alkaline earth metal citrate hydrates, which can be used as precursors – i.e. alkaline earth metal source – for various oxidic materials.[8,9]

For the alkaline earth metal citrates and citrate hydrates, only a surprisingly small number of crystal structures has been reported so far.[9,10,11–13] Regarding respective strontium compounds, $Sr_3(C_6H_5O_7)_2 \cdot 5H_2O$ is the only one with known crystal structure.[12] Moreover, $Sr_3(C_6H_5O_7)_2 \cdot 3.5H_2O$ can be found in literature with the water content being determined by thermogravimetry, only.[8]

Consequently, the strontium citrate monohydrate $Sr_3(C_6H_5O_7)_2 \cdot H_2O$ synthesized and characterized in this contribution has hitherto not been reported. According to our experiments it is only accessibly by hydrothermal conditions.

* Prof. Dr. H. A. Höppe
  E-Mail: henning@ak-hoeppe.de
[a] Lehrstuhl für Festkörperchemie, Institut für Physik
  Universität Augsburg
  Universitätsstraße 1
  86159 Augsburg, Germany

The employed microwave-assisted hydrothermal method provides significant advantages like straightforward preparation, mild reaction conditions, low cost and foremost short duration of syntheses.[14,15] Often, silicate-analogous strontium compounds are capable of substitution of Sr^{2+} by Eu^{2+} ions due to the ions' similar ionic radii [$r_{ion}(Sr^{2+})$ = 136 pm, $r_{ion}(Eu^{2+})$ = 135 pm][16] and same charge; therefore they are suited as hosts for luminescent Eu^{2+} materials, i.e. phosphors for white LED applications.[2,3] $Sr_3(C_6H_5O_7)_2 \cdot H_2O$ could be a promising precursor for the synthesis of such phosphors.

In this contribution, the first report on $Sr_3(C_6H_5O_7)_2 \cdot H_2O$ and its crystal structure based on single-crystal XRD data and a Rietveld refinement are given. For characterization, powder XRD, infrared spectroscopy and thermogravimetry were applied to elucidate its decomposition behavior as precursor material. For comparison and due to the lack of reported results, $Sr_3(C_6H_5O_7)_2 \cdot 5H_2O$ was prepared and investigated by the same methods – again with special interest on the compounds suitability as precursors.

Results and Discussion

Syntheses

$Sr_3(C_6H_5O_7)_2 \cdot H_2O$ was obtained via a microwave-assisted hydrothermal process starting from an aqueous solution of $Sr(NO_3)$ and $C_6H_8O_7$. The synthesis yielded a homogeneous colorless and phase-pure powder (Figure 1) including plate-like single crystals depicted in the SEM image in Figure 2. Energy dispersive X-ray (EDX) spectroscopy was used to determine the elemental composition (Figure S1, Supporting Information). The analysis clearly revealed the presence of solely strontium, carbon and oxygen. Herein, the Sr to C ratio gave 0.34 ± 0.05 and the Sr to O ratio 0.22 ± 0.03, which is in rela-

tively good agreement with the calculated ratios of 0.25 and 0.20, respectively. The deviations can be explained by a decreased accuracy of EDX spectroscopy for low atomic number elements such as carbon and oxygen.
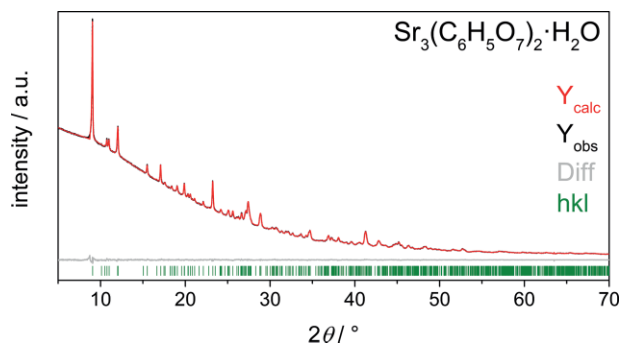
Figure 1. Rietveld-Refinement of $Sr_3(C_6H_5O_7)_2 \cdot H_2O$; further details can be found in Table S1 (Supporting Information); the comparison of the experimental pattern and a pattern calculated from the results of the single crystal structure determination can be found in Figure S2 (Supporting Information).
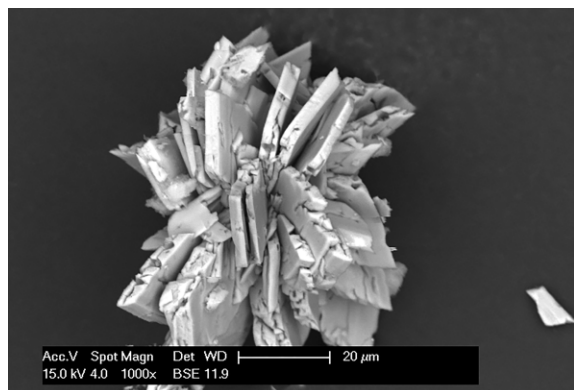
Figure 2. SEM image of as prepared $Sr_3(C_6H_5O_7)_2 \cdot H_2O$.

For comparison, $Sr_3(C_6H_5O_7)_2 \cdot 5H_2O$ was synthesized via precipitation from an aqueous solution of $SrCl_2$ and $Na_3C_6H_5O_7$ yielding also a colorless powder. The phase purity of both compounds was confirmed by powder X-ray diffraction (Figure 1, Figures S2 and S3, Supporting Information). Further, $Sr_3(C_6H_5O_7)_2 \cdot 5H_2O$ was dehydrated yielding a colorless powder which showed no crystalline order in the powder X-ray diffractogram. (Figure S4, Supporting Information) Consequently, only the FTIR spectrum of this sample was used for further interpretation.

Crystal Structure

$Sr_3(C_6H_5O_7)_2 \cdot H_2O$ crystallizes in space group $P\bar{1}$. Details of the structure determination are displayed in Table 1 and the crystal structure's unit cell is shown in Figure 3. The three strontium atoms occupy three lattice sites Sr(1), Sr(2) and Sr(3) and are coordinated by eight, nine and ten oxygen atoms, respectively. The coordination numbers are confirmed by calculations based on the MAPLE concept (Madelung Part of Lattice Energy).[17–19] The coordination environments of Sr(1),

Sr(2) and Sr(3) are depicted in Figure 4 and Figure S5 (Supporting Information). The $Sr(1)O_8$, $Sr(2)O_9$ and $Sr(3)O_{10}$ polyhedra are connected via either three or two common oxygen atoms, respectively. Hence, a three-dimensional network is formed. Due to the orientational disorder of one ligand (see below), Sr(3) is also disordered over two lattice sites with occupation factors of 83.0(2)% and 17.0(2)%, respectively. All Sr–O distances are reasonably close to the sum of ionic radii (Table 2) implying an ionic citrate–Sr bonding. By the citrate groups, Sr(1) is coordinated by two bidentate and four monodentate carboxylate groups, Sr(2) is coordinated by seven monodentate carboxylate groups and two hydroxyl groups, and Sr(3) is coordinated by three bidentate and three monodentate carboxylate groups plus one hydroxyl group in both the majority and the minority variant. The crystal water molecule does not coordinate directly to any Sr atom.

Table 1. Crystal data and structure refinements of $Sr_3(C_6H_5O_7)_2 \cdot H_2O$ determined from single-crystal X-ray diffraction [a].

	$Sr_3(C_6H_5O_7)_2 \cdot H_2O$
M /g·mol^{-1}	659.08
Crystal size /mm^3	$0.08 \times 0.04 \times 0.02$
Temperature /K	287(2)
Space group	$P\bar{1}$ (no. 2)
a /pm	1005.72(4)
b /pm	1015.06(5)
c /pm	1085.31(5)
α / °	89.642(2)
β / °	67.156(2)
γ / °	62.367(2)
Volume / 10^6 pm^3	883.85(7)
Z	2
$\rho_{calcd.}$ /g·cm^{-3}	2.476
Sbsorption coefficient μ /mm^{-1}	9.1
$F(000)$ / e	636
Radiation; wavelength λ /Å	Mo-K_α; 0.71073
Diffractometer	Bruker D8 Venture
θ range / °	2.318–24.799
Absorption correction	multi-scan
Transmission (min; max)	0.6014; 0.7453
index range hlkll	±11l±11l±12
Reflections collected	30895
Independent reflections	3040
Obs. reflections [$I > 2\sigma(I)$]	2659
Refined parameters / restraints	353 / 47
R_{int}	0.059
R_1	0.039
wR_2	0.066
GooF	1.054
Tesidual electron density (max; min) /e$^-$Å^{-3}	1.16; –0.88

a) The respective standard deviations are given in parentheses.

The coordination of the three Sr sites by the citrate groups is depicted in Figure S6 (Supporting Information). There are two different citrate groups both in trans/trans conformation, one of these shows oriental disorder; hereby, the substituents at the C-3 atom, i.e. the hydroxyl and carboxyl groups, change their positions in approx. a fifth of all cases as shown in Figure S7 (Supporting Information). This disorder also causes a respective disorder of one strontium atom. The conformation of the citrate anions in this work is in line with reports on alkali metal citrates with this conformation appearing for larger cat-
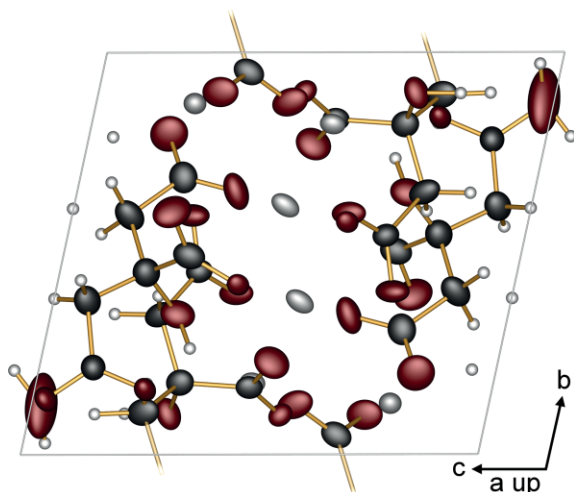
Figure 3. Perspective view of the unit cell of $Sr_3(C_6H_5O_7)_2 \cdot H_2O$; the Sr atoms are shown in light grey, oxygen in red, carbon in black and hydrogen in white; the displacement ellipsoids are set to 60% probability and hydrogen atoms are shown as simple spheres; only the majority component is shown for the sake of clarity.
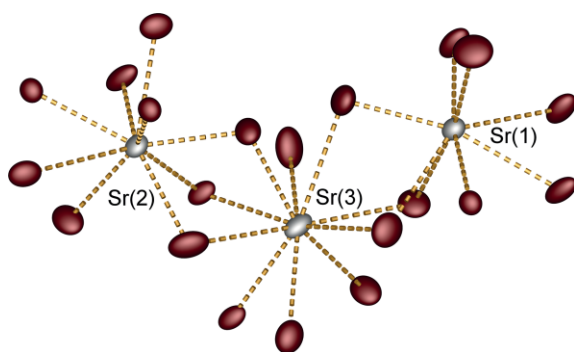
Figure 4. Coordination environments of the Sr^{2+} cations in $Sr_3(C_6H_5O_7)_2 \cdot H_2O$; the Sr atoms are shown in light grey, oxygen in red; the displacement ellipsoids are set to 60% probability; only the majority components of the orientational disorder are shown for the sake of clarity; the respective representation for the minority variant is depicted in Figure S5 (Supporting Information).

Table 2. Selected interatomic distances (in pm) and angles (in °) of $Sr_3(C_6H_5O_7)_2 \cdot H_2O$ [a].

Sr(1)–O	247(1)–291(6)
Sr(2)–O	247(5)–298.2(4)
Sr(3)–O [b]	249.7(4)–278.0(5)
Sr(3B)–O [c]	243.9(5)–279.2(5)
$\sum$ IR (Sr(1)–O)[17] [d]	261–264
$\sum$ IR (Sr(2)–O)[17] [d]	266–269
$\sum$ IR (Sr(3)–O)[17] [d]	271–274
C–O_c [e]	119(2)–128.0(8)
O–C–O	122.4(5)–125.9(7)
C–O_H [f]	137(2)–145.5(6)
C–C	152(2)–154(2)

a) The respective standard deviations are given in parentheses. b) Majority component. c) Minority component. d) Range of ionic radii sums due to oxygen with CN = 2, 3 and 4. e) O_c = oxygen as part of carboxylate group. f) O_H = oxygen as part of hydroxide group.

ions.[20] In the first citrate group, all three carboxylate groups coordinate one strontium bidentate and two strontium mono-

dentate each. In the majority disorder variant of the second citrate group one carboxylate group coordinates one strontium bidentate and two further strontium atoms monodentate, the second carboxylate group coordinates one strontium bidentate and one monodentate and the third carboxylate group coordinates two strontium atoms monodentate. In the minority variant two carboxylate groups are coordinating one strontium atom bidentate and two strontium atoms monodentate each, while the third carboxylate group coordinates two strontium atoms monodentate. Consequently, there is no non-coordinating oxygen atom in both citrate groups including the disordered variants.

The bond lengths and interatomic angles within the citrate groups depicted in Table 2 agree well with reports on other citrates and citric acid.[20,21] Within the carboxylate groups, the bond lengths are within the sum of ionic radii of 130 pm[16] implying a covalent bond alongside with O–C–O angles larger than 120° due to the charge.

The two citrate groups differ in the conformation of hydrogen bonds, too. The first citrate group's hydroxyl group forms a hydrogen bond to the crystal water molecule while the second exhibits intramolecular hydrogen bonds between the hydroxyl group and two carboxylate groups in the majority variant. The shorter distance to one carboxylate group is due to the respective oxygen atom being coordinated by two strontium atoms vs. the other carboxylate group's oxygen atom being bridging three strontium atoms. Further, intermolecular hydrogen bonds from the hydroxyl group to one methylene group of the first citrate group alongside with two hydrogen bonds of carboxylate groups with the crystal water molecule are formed in the majority variant. The minority component forms hydrogen bonds to the crystal water, only. However, the hydroxyl group is involved in the coordination of the strontium atoms. The hydrogen bond conformations are shown in Figure S8 (Supporting Information). Presumably due to the difference in hydrogen bonding, the hydroxyl group and the central carboxylate group lie in the same plane in the first citrate molecule, only.

Consequently, the citrate groups form an own three-dimensional network connected via hydrogen bonds. The complete crystal structure is constructed by the two interpenetrating Sr–O and citrate–water frameworks.

The crystal structure was confirmed by the Rietveld refinement on the powder diffraction data of $Sr_3(C_6H_5O_7)_2 \cdot H_2O$ summarized in Table S1 (Supporting Information) and displayed in Figure 1. The Rietveld refinement provides a slightly different set of lattice parameters founded on better statistics than the single crystal measurement.

The crystal structure of $Sr_3(C_6H_5O_7)_2 \cdot 5H_2O$ was reported by *Zacharias* and *Glusker*.[11] Here, there are also three Sr sites coordinated by 8, 9 or 10 oxygen atoms. The resulting Sr(1) O_9, Sr(2)O_8, Sr(3)O_{10} polyhedra are connected either via two or three oxygen atoms forming one dimensional chains. The Sr–O distances of 250–278 pm are slightly smaller than the ones found in $Sr_3(C_6H_5O_7)_2 \cdot H_2O$. The major difference between both structures are the coordinating crystal water molecules in $Sr_3(C_6H_5O_7)_2 \cdot 5H_2O$. Sr(1) is coordinated by two bi-

dentate and two monodentate carboxylate groups plus twice by crystal water and by one hydroxyl group. Sr(2) is coordinated by six monodentate carboxylate groups and two crystal water molecules, whereas Sr(3) is coordinated by two bidentate and two monodentate carboxylate groups plus one hydroxyl group and three crystal water molecules. Consequently, both citrate groups have two bidentate and one monodentate carboxylate group with one oxygen atom not coordinating any Sr atom. This oxygen atom is coordinated by hydrogen bonds towards the crystal water molecules.

Vibrational Spectroscopy

Infrared spectroscopy was performed on both $Sr_3(C_6H_5O_7)_2 \cdot H_2O$ and $Sr_3(C_6H_5O_7)_2 \cdot 5H_2O$ powders as well as on dehydrated $Sr_3(C_6H_5O_7)_2 \cdot 5H_2O$. The spectra shown in Figure 5 fit to published reports for similar compounds.[22–26] The presence or absence of crystal water is shown by the OH stretching vibration around 3400 cm^{-1}. Consequently, the dehydrated $Sr_3(C_6H_5O_7)_2 \cdot 5H_2O$ can be treated as $Sr_3(C_6H_5O_7)_2$ with a broad weak ν(OH) band remaining between 3400 cm^{-1} and 3200 cm^{-1} due to hydrogen bonds within the compound. The spectra are dominated by asymmetric carboxylate stretching modes around 1550 cm^{-1} and the symmetric carboxylate stretching modes between 1450 and 1400 cm^{-1}. The COH bending vibrations appear around 1080 cm^{-1} in all three spectra. This confirms the formation of $Sr_3(C_6H_5O_7)_2$ instead of $Sr_3(C_6H_3O_6)_2$ after the dehydration together with the ν(OH) bands around 520 cm^{-1}. CH$_2$ bending modes appear between 1330 and 1260 cm^{-1} and around 850 and 750 cm^{-1}. The weak C–C bending vibrations are located around 2950 and 1700 cm^{-1} with the former overlapping with C–H stretching modes. In $Sr_3(C_6H_5O_7)_2 \cdot 5H_2O$, the additional band around 1200 cm^{-1} is assigned to the additional bending mode within the carboxylate group due to one oxygen atom within the carboxylate group not coordinating a strontium cation. The Sr–O vibrations appear below wavenumbers of 450 cm^{-1} with more intensity in $Sr_3(C_6H_5O_7)_2 \cdot 5H_2O$ than in $Sr_3(C_6H_5O_7)_2 \cdot H_2O$ due to the shorter Sr–O distances shifting the band above 400 cm^{-1} and thus in the measured range.

Thermal Decomposition

The thermal decompositions of both, $Sr_3(C_6H_5O_7)_2 \cdot H_2O$ and $Sr_3(C_6H_5O_7)_2 \cdot 5H_2O$, were investigated by thermal analysis. For the monohydrate, the thermogravimetric (TG) curve shows three plateaus (see Figure 6). Firstly, one molecule H$_2$O is lost around 150 °C. Between 300 °C and 560 °C two steps overlap. Here, presumably the reactions from strontium citrate to strontium aconitate ($Sr_3(C_6H_3O_6)_2$) followed by the decomposition of $Sr_3(C_6H_3O_6)_2$ to SrCO$_3$ occur. The last step between 700 and 880 °C fits well with the decomposition of SrCO$_3$ to strontium oxide. The mass losses during the decomposition match well with the expected values of the suggested intermediates (Table S2, Supporting Information) and are in agreement with earlier reports on other alkaline earth citrate hydrates.[9,27–29]
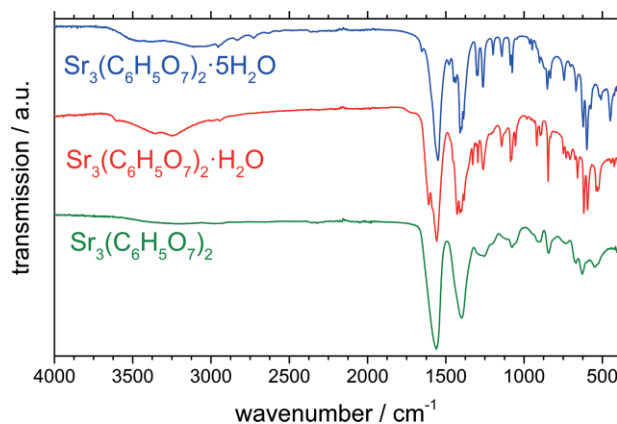
Figure 5. Infrared spectra of $Sr_3(C_6H_5O_7)_2 \cdot H_2O$, $Sr_3(C_6H_5O_7)_2 \cdot 5H_2O$ and dehydrated $Sr_3(C_6H_5O_7)_2 \cdot 5H_2O$ labelled $Sr_3(C_6H_5O_7)_2$.

Importantly, the first mass loss confirms the composition of the title compound as monohydrate.
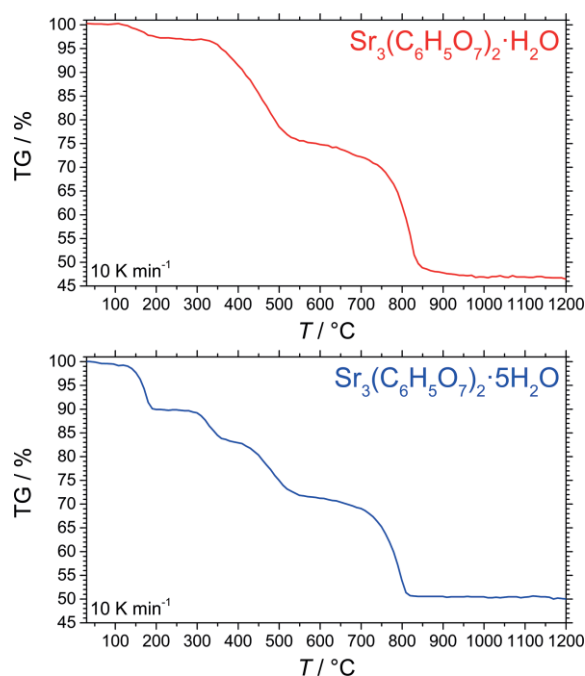
Figure 6. Thermal analysis of $Sr_3(C_6H_5O_7)_2 \cdot H_2O$ (top) and $Sr_3(C_6H_5O_7)_2 \cdot 5H_2O$ (bottom): the thermogravimetric (TG) curve is shown vs. temperature T.

The decomposition of the pentahydrate, $Sr_3(C_6H_5O_7)_2 \cdot 5H_2O$, follows a very similar sequence at almost the same temperatures (Figure 6 and Table S3, Supporting Information). There is no indication of the intermediate formation of the monohydrate during the first dehydration step. The formation of anhydrous $Sr_3(C_6H_5O_7)_2$ agrees well with the FT-IR spectrum of dehydrated $Sr_3(C_6H_5O_7)_2 \cdot 5H_2O$ (Figure 5). In contrast to $Sr_3(C_6H_5O_7)_2 \cdot H_2O$, the step towards strontium aconitate forms a distinct plateau. Furthermore, the mass losses for the formation of SrCO$_3$ and SrO deviate stronger from the calculated values than for $Sr_3(C_6H_5O_7)_2 \cdot H_2O$. This might be due to incomplete decomposition of $Sr_3(C_6H_3O_6)_2$ as reported

for respective calcium and barium citrate hydrates[28,30] or residual amorphous carbon. The formation of SrO is confirmed by powder X-ray diffraction (Figure S9, Supporting Information). Interestingly, $Sr(OH)_2$ as final product is a conceivable explanation of the experimentally observed mass loss. But this is in disagreement with literature reporting its decomposition and the formation of SrO above 700 °C and our powder X-ray diffraction results – so it is chemically highly improbable.[31]

Conclusions

In our contribution, strontium citrate monohydrate $Sr_3(C_6H_5O_7)_2 \cdot H_2O$ was prepared for the first time. Microwave-assisted hydrothermal syntheses yielded plate-like microcrystals. The compound was characterized using single crystal XRD, energy dispersive X-ray spectroscopy, powder XRD, vibrational spectroscopy and thermal analysis. The latter three were also applied to the hitherto only strontium citrate hydrate with known crystal structure, $Sr_3(C_6H_5O_7)_2 \cdot 5H_2O$.

$Sr_3(C_6H_5O_7)_2 \cdot H_2O$ represents a new structure type with two distinct citrate groups differing in the hydrogen bonding situation and the coordination towards the strontium atoms showing an orientational disorder of one citrate ligand. SrO_8, SrO_9 and SrO_{10} polyhedra are connected via either two or three common oxygen atoms. The crystal structure is formed by the combination of two interpenetrating Sr–O and citrate–crystal water frameworks.

$Sr_3(C_6H_5O_7)_2 \cdot H_2O$ may be used as a precursor for various strontium compounds. It can be synthesized easily and rapidly by microwave-assisted hydrothermal synthesis with a defined microcrystalline morphology being another advantage of this precursor. The same findings hold for $Sr_3(C_6H_5O_7)_2 \cdot 5H_2O$ showing very similar thermal behavior. However, the defined crystallinity is not achievable by easy synthesis. The preparation of crystalline anhydrous strontium citrate remains the objective of further investigations.

Experimental Section

Syntheses: $Sr_3(C_6H_5O_7)_2 \cdot H_2O$ (**1**): $Sr_3(C_6H_5O_7)_2 \cdot H_2O$ was prepared via a microwave-assisted hydrothermal synthesis. Firstly, 0.2 mmol $Sr(NO_3)_2$ (Fluka, >99%) and 0.2 mmol citric acid $C_6H_8O_7$ (Bernd Kraft, >99%) were dissolved in 1 mL deionized H_2O. The solution was filled in a borosilicate glass sample tube (10 mL) after stirring for 30 min (pH = 4). The tube was sealed, placed in a microwave reactor (CEM, Discover S) and heated to 130 °C at 80 W for 60 min. After cooling to room temperature, the product was separated and washed by centrifugation at 4000 rpm for 10 min two times with deionized water and once with ethanol. Subsequently, the product was dried in a compartment dryer at 65 °C for 24 h and obtained with a yield of 11% with respect to the employed strontium amount.

$Sr_3(C_6H_5O_7)_2 \cdot 5H_2O$ (**2**) was synthesized via precipitation from an aqueous solution. 2.05 mmol $SrCl_2 \cdot 6H_2O$ (Merck, >99%) and 1.37 mmol $Na_3C_6H_5O_7 \cdot 2H_2O$ (Aldrich, >99%) were dissolved in 50 mL deionized H_2O and stirred while heating at 100 °C for 30 min. The resulting precipitate was vacuum-filtered along with washing with additional 50 mL H_2O, then 50 mL Ethanol and finally dried in air at

ambient conditions yielding 79% with respect to the employed strontium amount.

Furthermore, $Sr_3(C_6H_5O_7)_2 \cdot 5H_2O$ (**2**) was dehydrated. The sample was heated at 160 °C in a corundum crucible inside a tube furnace with 90 mL min^{-1} nitrogen flow for 12 h with heating ramps of 80 K·h^{-1}. Moreover, $Sr_3(C_6H_5O_7)_2 \cdot 5H_2O$ was heated at 1200 °C in a corundum crucible inside a muffle furnace for 10 h with heating ramps of 200 K·h^{-1} in order to investigate the thermal decomposition product.

EDX Spectroscopy/SEM: The elemental composition of solid $Sr_3(C_6H_5O_7)_2 \cdot H_2O$ (**1**) was confirmed by energy dispersive X-ray (EDX) spectroscopy with a Philips XL 30 FEG scanning electron microscope (SEM) equipped with an EDAX SiLi detector (average of three measurements).

Single Crystal Structure Determination: Suitable single crystals of $Sr_3(C_6H_5O_7)_2 \cdot H_2O$ were selected for single-crystal XRD under a polarizing microscope. Diffraction data were collected with a Bruker D8 Venture diffractometer using Mo-K_α radiation (λ = 0.7093 Å). Absorption correction was performed by the multi-scan method. The structures were solved by Direct Methods and refined by full-matrix least-squares technique with the SHELXTL crystallographic software package.[32] During the refinement we recognized a significant residual electron density near Sr(3) pointing towards a disorder; further residual electron densities around the second citrate ligand [C(7)···C(12)] confirmed this estimation. Without considering this disorder the wR_2 converged around 0.12; the refinement of the heavy-atom disorder led to the discovery of a further orientation of the second citrate ligand where the substituents at C-3 (hydroxyl and carboxyl groups) are exchanged yielding an orientational disorder of approx. 180°; both orientations were related to each other by SAME and EADP commands, the hydrogen atoms of the minority orientation were refined employing a riding model (HFIX) of the CH_2 groups and identified by residual electron density for the OH group. Considering this disorder led to wR_2 of 0.066 with volume contributions of 83.0(2)% (majority orientation) and 17.0(2)% (minority). For the majority components of this disorder the hydrogen atoms were refined using residual density of electrons for localization and a reasonable restraint for the length of the O–H bonds.[33] All hydrogen atoms were assigned fixed isotropic displacement parameters equal to $1.2U_{eq}$ of the bonded oxygen or carbon atom within the OH or CH_2 groups and $1.5U_{eq}(OW)$ in H_2O, respectively. Moreover, the occupation of the crystal water molecule was refined freely yielding full occupation within the margins of error – and fixed to full occupation for the last refinements to stabilize the cycles. Relevant crystallographic data and further details of the structure determinations are summarized in Table 1.

Further details of the crystal structure investigations may be obtained from the Fachinformationszentrum Karlsruhe, 76344 Eggenstein-Leopoldshafen, Germany (Fax: +49-7247-808-666; E-Mail: crysdata@fiz-karlsruhe.de, http://www.fiz-karlsruhe.de/request for deposited data.html) on quoting the depository number CSD-1986186.

X-ray Powder Diffraction: The $Sr_3(C_6H_5O_7)_2 \cdot H_2O$ (**1**) sample was ground and filled into a Hilgenberg glass capillary (outer diameter 0.3 mm, wall thickness 0.01 mm). The data were collected with a Bruker D8 Advance diffractometer with Cu-K_α radiation (λ = 1.54184 Å) with a 1D LynxEye detector, steps of 0.02° and transmission geometry.

The $Sr_3(C_6H_5O_7)_2 \cdot 5H_2O$ (**2**) sample was measured with a Seifert 3003 TT diffractometer at room temperature in Bragg–Brentano geometry using Cu-K_α radiation (λ = 1.54184 Å), a GE METEOR 1D line detec-

tor and a Ni-Filter to suppress Kβ radiation (X-ray tube operated at 40 kV and 40 mA, scan range: 5–80°, increment: 0.02°, 40 scans per data point, integration time: 200 s per degree, variable divergence slit).

Rietveld Refinement: Analysis of diffraction data was performed using the Rietveld method with the program TOPAS V. 5.0.[35] The instrumental resolution function was determined empirically from a set of fundamental parameters using a reference scan of Si (NIST 640d).[35] The structural model of $Sr_3(C_6H_5O_7)_2 \cdot H_2O$ from our single crystal XRD measurement of the majority orientation of the second citrate ligand was used as a starting model for Rietveld analysis of $Sr_3(C_6H_5O_7)_2 \cdot H_2O$ measured at room temperature to stabilize the refinement. The isotropic thermal displacement parameters were constrained to one common value for all strontium atoms and another one for all carbon and oxygen atoms in order to minimize quantification errors. Analogously to the single crystal structure determination, the isotropic thermal displacement parameters of the hydrogen atoms were set to 1.2 or 1.5 times the common value of C and O for OH or CH_2 groups and H_2O, respectively. Details of the refinement are displayed in Table S1 (Supporting Information).

FT-IR Spectroscopy: The Fourier-transform infrared spectra were recorded at room temperature with a Bruker EQUINOX 55 T-R spectrometer using a Platinum ATR device (scan range: 400–4000 cm^{-1}, resolution: 2 cm^{-1}, 32 scans per sample).

Thermogravimetry: Thermogravimetric analyses (TGA) were performed with a NETZSCH STA/TG 409 PC Luxx thermobalance in a nitrogen atmosphere (flow rate: 70 mL·min^{-1}) in corundum crucibles (heating rate: 10 K·min^{-1}). Attempts to investigate the thermal decomposition products by variable-temperature powder X-ray diffraction were unsuccessful due to a loss of crystalline order during the decomposition of both samples.

Supporting Information (see footnote on the first page of this article): EDX spectra, Powder XRD pattern, additional structure graphics, Rietveld refinement details, experimental and theoretically predicted mass losses of thermal analysis.

References

[1] P. Netzsch, M. Hämmer, P. Gross, H. Bariss, T. Block, L. Heletta, R. Pöttgen, J. Bruns, H. Huppertz, H. A. Höppe, *Dalton Trans.* **2019**, *48*, 4387–4397.

[2] H. A. Höppe, M. Daub, M. C. Bröhmer, *Chem. Mater.* **2007**, *19*, 6358–6362.

[3] M. J. Schäfer, S. G. Jantz, H. A. Höppe, *Z. Naturforsch. B* **2020**, *75*, 143–148.

[4] P. Netzsch, P. Gross, H. Takahashi, S. Lotfi, J. Brgoch, H. A. Höppe, *Eur. J. Inorg. Chem.* **2019**, 3975–3981.

[5] M. Hämmer, H. A. Höppe, *Z. Naturforsch. B* **2019**, *74*, 59–70.

[6] P. Gross, H. A. Höppe, *Chem. Mater.* **2019**, *31*, 8052–8061.

[7] A. M. Kaczmarek, K. van Hecke, R. van Deun, *Chem. Soc. Rev.* **2015**, *44*, 2032–2059.

[8] S. Guillemet-Fritsch, H. Coradin, A. Barnabé, C. Calmet, P. Tailhades, A. Rousset, *MRS Proc.* **2001**, *674*, 127.

[9] E. Herdtweck, T. Kornprobst, R. Sieber, L. Straver, J. Plank, *Z. Anorg. Allg. Chem.* **2011**, *637*, 655–659.

[10] J. A. Kaduk, *Powder Diffr.* **2018**, *33*, 98–107.

[11] D. E. Zacharias, J. P. Glusker, *Acta Crystallogr., Sect. C* **1993**, *49*, 1732–1735.

[12] B. Sheldrick, *Acta Crystallogr., Sect. B* **1974**, *30*, 2056–2057.

[13] C. K. Johnson, *Acta Crystallogr.* **1965**, *18*, 1004–1018.

[14] K. Byrappa, T. Adschiri, *Prog. Cryst. Growth Charact. Mater.* **2007**, *53*, 117–166.

[15] L.-Y. Meng, B. Wang, M.-G. Ma, K.-L. Lin, *Mater. Today Chem.* **2016**, *1–2*, 63–83.

[16] R. D. Shannon, *Acta Crystallogr., Sect. A* **1976**, *32*, 751–767.

[17] R. Hoppe, *Angew. Chem.* **1966**, *78*, 52–63.

[18] R. Hoppe, *Angew. Chem. Int. Ed. Engl.* **1970**, *9*, 25–34.

[19] R. Hübenthal, MAPLE, Program for the Calculation of the Madelung Part of Lattice Energy, Universität Gießen, Gießen **1993**.

[20] A. Rammohan, J. A. Kaduk, *Acta Crystallogr., Sect. B* **2018**, *74*, 239–252.

[21] J. P. Glusker, J. A. Minkin, A. L. Patterson, *Acta Crystallogr., Sect. B* **1969**, *25*, 1066–1072.

[22] P. Tarakeshwar, S. Manogaran, *Spectrochim. Acta Part A* **1994**, *50*, 2327–2343.

[23] K. Nakamoto, *Infrared and Raman Spectra of Inorganic and Coordination Compounds*, 6th ed., Wiley-Blackwell, Oxford **2008**.

[24] A. Drzewiecka-Antonik, A. E. Koziol, P. Rejmak, K. Lawniczak-Jablonska, L. Nittler, T. Lis, *Polyhedron* **2017**, *132*, 1–11.

[25] M. Matzapetakis, N. Karligiano, A. Bino, M. Dakanali, C. P. Raptopoulou, V. Tangoulis, A. Terzis, J. Giapintzakis, A. Salifoglou, *Inorg. Chem.* **2000**, *39*, 4044–4051.

[26] Y. Gao, P. Zhang, J. Li, J. Cao, X. Lai, L. Zhong, *Micro Nano Lett.* **2015**, *10*, 419–421.

[27] S. A. A. Mansour, *Thermochim. Acta* **1994**, *233*, 231–242.

[28] S. A. A. Mansour, *Thermochim. Acta* **1994**, *233*, 243–256.

[29] M. M. Barbooti, D. A. Al-Sammerrai, *Thermochim. Acta* **1986**, *98*, 119–126.

[30] A. Srivastava, P. Singh, V. G. Gunjikar, C. I. Jose, *Thermochim. Acta* **1984**, *76*, 249–254.

[31] R. Dinescu, M. Preda, *J. Therm. Anal.* **1973**, *5*, 465–473.

[32] G. M. Sheldrick, *Acta Crystallogr., Sect. C* **2015**, *71*, 3–8.

[33] T. Steiner, *Angew. Chem. Int. Ed.* **2002**, *41*, 48–76.

[34] Bruker AXS, Topas V5, General profile and structure analysis software for powder diffraction data. User's Manual, Karlsruhe, Germany **2014**.

[35] R. W. Cheary, A. A. Coelho, J. P. Cline, *J. Res. Natl. Inst. Stand. Technol.* **2004**, *109*, 1–25.

Z. Anorg. Allg. Chem. **2021**, 204–209   **www.zaac.wiley-vch.de**   **209**